Journal of Hazardous Materials 165 (2009) 206–217

Contents lists available at ScienceDirect

Journal of Hazardous Materials

journal homepage: www.elsevier.com/locate/jhazmat

Nickel–iron layered double hydroxide (LDH): Textural properties upon hydrothermal treatments and application on dye sorption

Fatiha Boukraa Djellal Saiah[a,*], Bao-Lian Su[b], Nourredine Bettahar[a]

[a] Laboratory of Physics-Chemistry of Materials (L.P.C.M): Catalyse and Environment, University of Sciences and Technology of ORAN "Mohamed Boudiaf" (USTO.MB), B.P. 1505 El Menaouer, Oran 31000, Algeria
[b] Laboratory of Inorganics Materials Chemistry (CMI), University of Namur (FUNDP), 61 Rue de Bruxelles, B-5000 Namur, Belgium

ARTICLE INFO

Article history:
Received 4 May 2008
Received in revised form 7 July 2008
Accepted 25 September 2008
Available online 15 October 2008

Keywords:
Anionic clays
Hydrothermal treatment
Crystallinity
Textile dye
Adsorption

ABSTRACT

$NiFeCO_3$ hydrotalcites with Ni/Fe molar ratio of 3 were synthesized by co-precipitation method at constant pH, followed by hydrothermal treatment at various temperatures 85–180 °C for 3–360 h. The obtained materials were characterized by XRD analysis, FT-IR spectroscopy, SEM and TEM microscopy, TGA and BET techniques. The resulting materials were found to be similar to the hydrotalcite with a well-defined hexagonal morphology of crystallites. The hydrothermal treatment and aging time increases the platelet sizes and decreases the surface area. XRD analysis showed the formation of sharper and intense peaks, which might indicate the larger crystallites size of LDH as well as higher crystallinity. Furthermore, textural studies revealed influence of aging time and temperature on the properties of the crystalline phase. The prolonged time tends to form additional products, identified as $NiFe_2O_4$ spinel and NiO nickel oxide.

The effect of hydrothermal treatment temperature on the kinetics of dye removal has been explored. It was found that the percentage color removal increases with increasing hydrothermal treatment temperature up to 140 °C and aging time up to 4 days. Furthermore, the color removal decreases with increasing hydrothermal treatment temperature up to 140–180 °C and prolonged aging time.

1. Introduction

Hydrotalcite (HT) belongs to the class of anionic clay minerals, known as layered double hydroxides (LDHs). These LDHs represent one of the most technologically promising materials because of their relative ease of preparation and broad use as adsorbents, anion exchangers [1–3], catalysts [4] and catalyst supports [5,6]. Although for application in medicine [7] environmental protection [8], pharmaceutical applications [9] and cosmetic [10] LDH containing Mg^{2+} and Al^{3+} are usually preferred because of their lack of toxicity, those with transition metal cations are generally used as catalysts [4–6]. They can be described as layered compounds of brucite-like structure ($Mg(OH)_2$). The general formula: $\left[M^{2+}_{1-x}M^{3+}_{x}(OH)_2\right]^{x+}\left[A^{n-}_{x/n}\cdot mH_2O\right]^{x-}$, where M^{2+} and M^{3+} can be any divalent and trivalent cation in the octahedral positions within the hydroxide layers: $M^{2+}=Mg^{2+}$, Zn^{2+}, Ni^{2+}, etc., and the metal ratio $x=M^{3+}/(M^{2+}+M^{3+})$ variable ($0.2<x<0.33$). Their structure consists of positively charged brucite-like layers, $\left[M^{2+}_{1-x}M^{3+}_{x}(OH)_2\right]^{x+}$, alternating with negatively charged inter layers containing anions and water molecules $\left[A^{n-}_{x/n}\cdot mH_2O\right]^{x-}$ [11,12] (Fig. 1). There is no limitation on the nature of the anion provided it does not form a complex with the cations [1]. The wide range of synthetic materials of this type shows an extensive range of properties. An increasing attention has been drawn to these compounds owing to the diverse applications. However, the nature of applications is influenced by optimum physicochemical properties in particular by crystallinity, surface, texture and particle size. Various methods have been reported as salt oxide method [13], co-precipitation [14], induced hydrolysis [15], reconstruction [16] and anion-exchange [17] to synthesize these compounds with altered physicochemical characteristics. However, co-precipitation at fixed pH is the most commonly used materials. Therefore, studies of the crystal chemistry of hydrotalcite-like compounds have mainly focused on the influence of their composition on lattice parameters and on physical properties [18]. Although there is still profuse interest in the ability to increase particle size. Layer crystals are better for characterization. However, bigger crystals have been produced by applying a temperature gradient to allow the rate of growth to be controlled [19]. Hydrothermal treatment generally increases crystallinity, depending mainly on temperature, although pressure and time are also important parameters. Miyata found, by hydrothermally treating an Mg/Al hydrotalcite, that the temperature had a

* Corresponding author. Tel.: +213 790540163; fax: +213 41560188.
E-mail address: f_boukraa2003@yahoo.fr (F.B.D. Saiah).

0304-3894/$ – see front matter © 2009 Published by Elsevier B.V.
doi:10.1016/j.jhazmat.2008.09.125

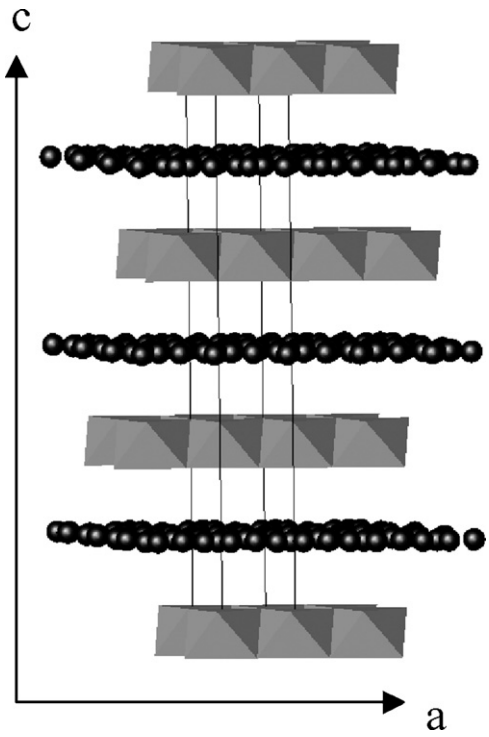

Fig. 1. The hydrotalcite structure. Grey octahedral: brucite-type layers, black dots: interlayer water and carbonate.

dramatic effect on crystallite size, such that size increased up to 180 °C but decreased above 200 °C [20]. A more recent study by X-ray diffraction and infrared spectroscopy, investigates the effect of varying time at constant temperature [21] and found that, the order in the inter layer region and the crystallinity in the hydroxide layer increased with time. Furthermore, transmission electron microscopy shows that the average size of the lamellar hexagonal particles increased with aging time [21].

Of particular importance to potential application is a reproducible control of the microstructure and composition of the material, we have studied the structural characteristics of some of nickel–iron samples which have been synthesized and hydrothermally treated at different temperature at various aging time. It is expected that different physical and chemical characteristics depend on the hydrothermal treatment route used, in particular, crystallinity, surface area, porosity, and purity can all vary. Such variables will influence the potential application and catalytic properties of the final materials.

Among the different pollutant of aquatic ecosystems, dyes are large and important groups of industrial chemicals [22]. Most of this were used in the textile industry and the dyes used include many different compounds which their environmental behavior is mainly unknown [23]. Interest in the environmental behavior of dyes is prompted primarily by concern over their possible toxicity and carcinogenicity, heightened by the fact that many dyes formerly were made of known carcinogens such as benzidine, which may be reformed. As a result of metabolism [22,23]. Disperse dyes have been shown to have high partition coefficients and solubility, suggesting significant potential for bioconcentration [24]. Most dyestuffs are designed to the resistant to environmental conditions like sunlight, effects of pH and microbial attack [25]. Hence, their presence in waste water is unwarranted, and it is desirable to remove coloring material from effluents, before their discharge to the environment. This is important to regions where water resources might be scarcer or sensitive.

The purpose of this work is to study the effect of hydrothermal treatment conditions on structural and textural properties of synthetic Ni/Fe-CO_3 LDH. This effect is also investigated on the removal efficiency and adsorption capacity of dye onto Ni/Fe-CO_3 LDH.

Ni/Fe-CO_3 LDH with molar ratio of 3 was synthesized using a co-precipitation method at constant pH. The samples were examined on the basis of purity, crystallinity and textural properties. However, we tried to optimize the conditions of the hydrothermal treatment in order to obtain a pure and well crystallized hydrotalcite phase. Hydrothermal treatment conditions is applied to improve the crystallinity [26] and the removal efficiency of a commercial dye Evan's Blue (Blue direct 53) on $NiFeCO_3$ LDH.

2. Experimental

2.1. Preparation

All reactants used in this work have high purity degree and were from Aldrich. A co-precipitation method was used to prepare $NiFeCO_3$ LDHs with a molar ratio Ni/Fe = 3 and the materials has submitted different hydrothermal treatment conditions. In a typical synthesis, the samples were obtained by dropwise adding, at room temperature, a solution containing 1.5 mol $NiCl_2{\cdot}6H_2O$ and 0.5 mol $FeCl_3{\cdot}6H_2O$ dissolved in 250 ml of distilled water to a vigorously stirred solution (250 ml) containing NaOH (1 M) and Na_2CO_3 (2 M) at constant pH = 11. The suspension obtained (yellow brown precipitate) was stirred mechanically for a further 1 h at room temperature during which time the pH value was still maintained constant. The suspension was then divided into several equal portions, to undergo different hydrothermal treatment. The content was then transferred into the teflon coated stainless steel autoclave in order to obtain better crystallized materials [15]. These portions denoted HT-85 and HT-180 were aged at 85 °C to 180 °C for 3 h to 15 days. After the hydrothermal treatment, the precipitate formed was filtered and washed several time with distilled water to remove excess soluble ions, until the filtrate pH was 7. The washed precipitate was dried in an oven at 60 °C overnight and the product obtained has different colors, from green to the green-brown according to the hydrothermal treatment conditions.

2.2. Sorption of Evan's Blue (EB)

2.2.1. Analytical technique

Evan's Blue (denoted EB) $C_{34}H_{24}N_6Na_4S_4O_{14}$, 99% purity was from Aldrich and used as received. The chemical structure of EB is shown in Fig. 2. It is an acid dye of the diazo series. The calibration curve for the dye was prepared by recording the absorbance values for a range of known concentrations of dye solutions at the wavelength of maximum absorbance (λ = 605 nm).

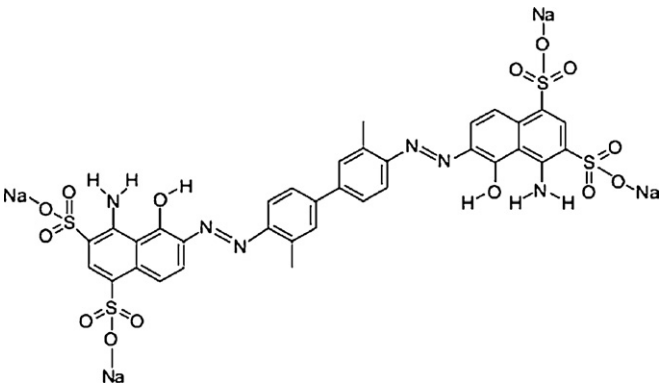

Fig. 2. Chemical structure of Evan's Blue (EB) dye.

2.2.2. Effect of contact time

A sorption kinetic study of Evans Blue (EB) on nickel–iron LDH was carried out by adding 250 mg of $NiFeCO_3$ LDH into 100 ml of EB solution at concentration about 50 mg/l. The mixture was stirred at room temperature. An approximately 5 ml of the solution was withdrawn at a desired time intervals, ranging from 2 to 70 min, and then centrifuged at 6500 rpm for 10 min, and diluted to 50 ml. Aliquots of the supernatant were also centrifuged at 6500 rpm for 10 min then EB equilibrium concentration was determined by employing the absorbance calibration curve using a Perkin–Elmer UV–Vis spectrometer at λ_{max} = 605 nm and the results were recorded as percent dye removal versus time. These conditions hold for all materials displayed above. So, the effects of hydrothermal treatment temperature on EB sorption were also investigated.

2.3. Characterization

Powder X-ray diffraction patterns (XRD) of synthesized LDHs were recorded using Philips PW1820 with Cu K_α radiation (λ = 1.5418 Å at a scan speed of 0.02° s) over a 2θ range of 4–70°. Identifications of the crystalline phases were done by comparison with the JCPDS files [27]. FT-infrared spectra of materials were recorded using KBr pellets technique in a PerkinElmer FT-IR 2000 spectrometer in the range of 4000–400 cm^{-1}. Specific surface area of Ni/Fe LDH samples at different hydrothermal treatment temperatures and time was measured in a Micromeritics Tristar 3000 by nitrogen adsorption N_2 (77 K) after degassing the sample in a vacuum by flowing nitrogen overnight at 100 °C. The surface areas were determined by applying BET method in the nitrogen adsorption data. The pore diameter and the pore size distribution were determined by the BJH method [28]. The morphology of the obtained phases was studied using Philips XL-20 scanning electron microscope (SEM) at 20 keV. Electron micrographs of the samples were taken by the transmission electron microscopy (TEM) on Philips TECNAI-10 instrument at 80 keV. Thermogravimetric/Differential Scanning Calorimetry (TG/DSC) of these materials was carried out using Seteram TG-DSC111 equipment, in the temperature range between 20 and 650 °C at a heating rate of 5 °C min^{-1} under a nitrogen atmosphere. Hereafter, the samples are indicated by the hydrothermal treatment time followed by hydrothermal treatment temperature, for example, NiFe4d120 indicates the treatment time is 4 days prepared under hydrothermal treatment temperature of 120 °C respectively, or NiFe12h160 indicates the treatment time is 12 h prepared under hydrothermal treatment temperature of 160 °C respectively.

3. Results and discussion

After drying, the color of the material should show a significant graduation of color intensity depending on the hydrothermal treatment temperature and time. The samples color was green up to 140 °C treated for 7 days, and the samples treated at higher temperature and time are rather green-brown.

3.1. XRD analysis

Powder X-ray diffraction patterns of $NiFeCO_3$ LDH at different hydrothermal treatment temperatures for various times are shown in Fig. 3. The patterns of all samples showed the diffraction lines typical for hydrotalcite structure with interlayer carbonate [24]. All samples demonstrate its layered structure. However, the hydrothermal treatment conditions have proved to be very limited to lead to pure materials, it is probably due to the particular mechanism of formation of LDH according to the treatment conditions. So it has been shown that NiFe(8-12h)180 (Fig. 3A), NiFe(1-15d)160 (Fig. 3B) and NiFe15d140 (Fig. 3C) presented co-forming of additional amorphous phases, which the diffraction lines increase with increasing the hydrothermal temperature and time. Then this effect is important for high treatment temperature, becoming more evident when the hydrothermal treatment is prolonged. As shown in Fig. 3, the XRD patterns of LDH samples consists of both sharp and symmetrical peaks with some asymmetrical peaks at high angle, indicating good crystallinity [25,26]. The sharpness of the narrow peaks increase, as the hydrothermal treatment increase at high temperature, indicating an improved crystallinity and a larger crystallite size.

Table 1
PXRD results for $NiFeCO_3$ hydrotalcite (Å).

NiFe4d85	NiFe7d140	NiFe15d160	Ref. [29]	Ascription (hkl)
7.727	7.755	7.857	7.717	003 H
			4.806	111 S
		4.611		001 NH
3.834	3.857	3.894	3.845	006 H
		2.969	2.956	220 S
		2.709		100 NH
2.677	2.688	2.682	2.661	101 H
2.609	2.598	2.617	2.587	012 H
		2.532	2.525	311 S
			2.412	222 S
2.329	2.338	2.335	2.321	015 H
		2.103	2.090	400 S
1.949	1.936	1.948	1.920	018 H
			1.710	10*10* H, 422 S
		1.743		400 S
		1.612	1.608	10*11* H, 511 S 333 S
		1.561		110 NH
1.544	1.549	1.547	1.541	110 H
1.518	1.518	1.516	1.511	113 H
		1.477	1.476	10*13* H, 440 S
				110 O
1.434	1.437	1.438	1.430	116 H
			1.410	531 S

H: hydrotalcite; S: $NiFe_2O_4$ spinel; NH: $Ni(OH)_2$ nickel hydroxide; O: NiO nickel oxide. Positions of lines are given in (Å).

The XRD patterns give two or three sharp peaks which show some common features of layered materials such as narrow and symmetric, strong peaks at low 2θ values, corresponding to the basal spacing and higher order diffractions, and weaker less symmetric lines at high 2θ values. Positions (in Å) of the maxima and the ascription to the corresponding (*h k l*) planes are given (Table 1) for the samples NiFe4d85, NiFe7d140 and NiFe15d160. del Arco et al. [29] have reported XRD results of sample $NiFeCO_3$ hydrothermally treated at 100 °C for 6 days, as in Table 1. The positions and relative intensities of the maxima for our samples are coincident with those reported in the literature for $Ni_{0.75}Fe_{0.25}(CO_3)_{0.125}(OH)_2 0.38H_2O$ (JCPDS file 40-0215) [30]. The cell constant "*c*" is commonly calculated as $c = 3d(0\,0\,3)$, assuming a 3R polytipism for the hydrotalcite [31,32], while the value of cell constant "*a*" is calculated as $a = 2d(1\,1\,0)$ [33] and the values calculated are given in Table 2. However, in the PXRD diagram of sample NiFe15d160, some lines cannot be ascribed to the hydrotalcite structure and, from comparison of the data with those reported in the JCPDS tables for hydrotalcite and the calcined samples, it was concluded that they correspond to a $NiFe_2O_4$ spinel phase and to NiO phase. Three strongest reflections lines, for which the maxima of peaks are recorded at 2θ = 19.28° due

Table 2
Experimental spacing (Å) for diffraction lines (0 0 3) of the samples, their ascription, and lattice parameters *a* and *c* (Å).

Samples	*a*	*c*	*d* (0 0 3)
NiFe4d85	3.088	23.18	7.727
NiFe7d140	3.098	23.26	7.755
NiFe15d160	3.094	23.57	7.857

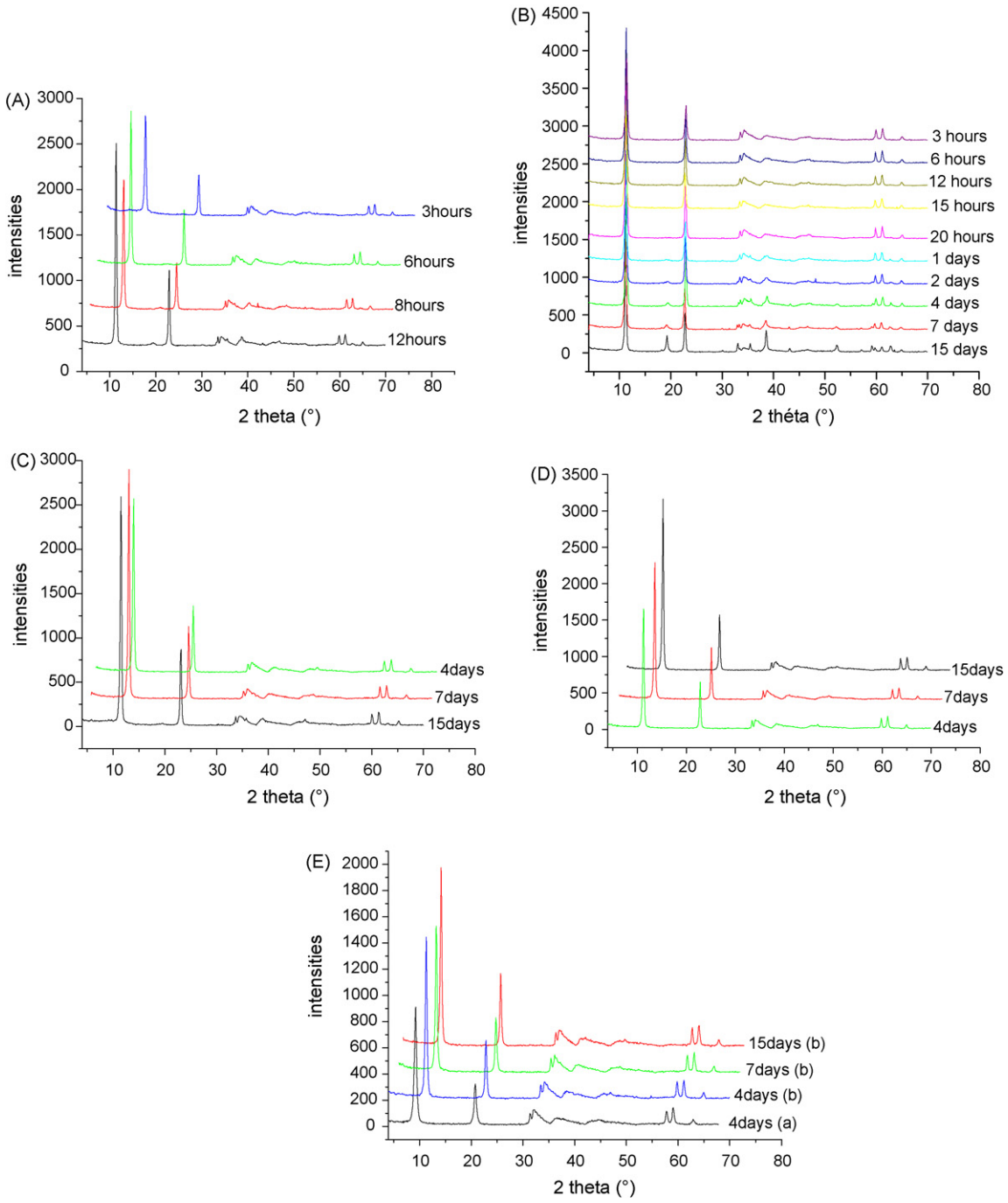

Fig. 3. X-ray diffraction patterns of NiFeCO3 LDHs at different hydrothermal treatment temperature and times: (A) at 180 °C, (B) at 160 °C, (C) at 140 °C, (D) at 120 °C and (E): (a) at 85 and (b) at 100 °C for various times.

to plane (0 0 1), at $2\theta = 33.12^\circ$ due to plane (1 0 0), and at $2\theta = 38.61^\circ$ due to plane (1 0 1) correspond to $Ni(OH)_2$ nickel hydroxide (JCPDS file 14-0117) (Fig. 3A and B). Weak reflections showed a trace of nickel hydroxide phase in the sample NiFe15d140 (Fig. 3A). In addition, these peaks are completely absent or reduced in their intensity as the hydrothermal treatment time decreased as in Fig. 3A and B. The values for parameter "*a*" are nearly constant for all samples as in Table 2. This parameter corresponds to the minimum cation–cation distance in the brucite-like layers and is related to position of the peak due to planes (1 1 0). On the other hand, it is observed that the *d*-spacing values increased between the temperatures 85 and 160 °C, giving rises to increasing parameter "*c*" as the hydrothermal temperature and time increased. It has been explained by a structural rearrangement and probably a better packing of the layers introduced by the hydrothermal treatment conditions. It is important to note that the variation of the basal spacing can be changed by means of hydrothermal treatment conditions. This means a consequence that we would be able to design materials with desirable pore sizes in the mesopore region, which is valuable in reaction catalysis and in adsorption [34].

3.2. Infrared analysis

The infrared absorption spectrum of the hydrotalcite samples of Ni/Fe at different hydrothermal treatment temperature and time are shown in Fig. 4A and B. For the infrared analysis of these layer

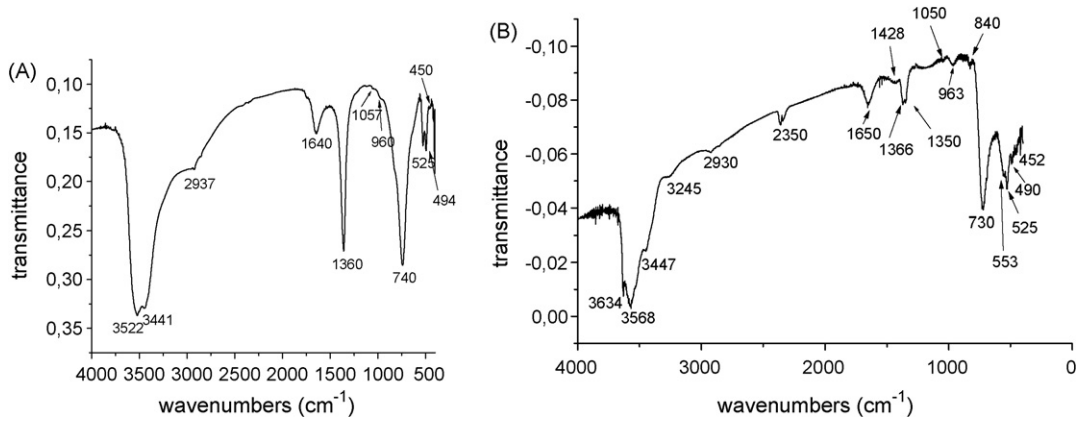

Fig. 4. FT-IR spectra of $NiFeCO_3$ LDH: (A) NiFe4d140 and (B) NiFe15d160.

hydroxides, vibrations can be approximately separated into those of the constituents units, i.e., vibrations of the interlayer anions, the hydroxyl groups (molecular vibrations) and the octahedral layers (lattice vibrations) [35]. It showed a broad band between 4000 and 3000 cm^{-1} (Fig. 4A and B), three broad and intense bands are observed, which are attributed to the twisting vibrations of physisorbed water, vibrations of the structural OH^- groups, characteristic valency vibrations of OH···OH, and/or characteristic stretching vibrations of M–OH in hydroxycarbonates. The FT-IR spectra of all $NiFeCO_3$ samples were quite similar though some differences were noticed in the intensity and broadness of the bands. The band centred around 3600 and 3500 cm^{-1} is assigned to a complex of overlapping stretching modes of the hydroxyl groups present, both those in the brucite-type layer (Ni/Fe–OH) and the interparticle and interlayer water molecules. The bands at 2937 and 3441 cm^{-1} are assigned to the CO_3–H_2O bridging mode and ν_{OH} mode of free and hydrogen-bonded hydroxyl groups and water molecule, respectively [36], whose bending mode is responsible for the medium-intensity band at 1630 cm^{-1}. The split bands with maxima at 1428 and 1366 cm^{-1} (Fig. 4B) should be ascribed to the antisymmetric stretching mode of CO_3^{2-} species, recorded as a single band at 1450 cm^{-1} for free CO_3^{2-} species, but which split because of the lower symmetry in the interlayer space, probably due to hydrogen bonding with OH groups and/or H_2O molecules. The values found here for the position of this split bands are very close to those reported by Hernandez-Moreno et al. [37] for Al–Li hydrotalcite materials and Labajos et al. [15] for Mg–Al hydrotalcite materials. Such a symmetry lowering also gives rise to activation of the IR-forbidden ν_1 mode of CO_3^{2-} species, thus accounting for the shoulder absorption band 1062 and 1050 cm^{-1} (Fig. 4A and B). This band is even weaker and hardly recorded in the other hydrotalcite samples, probably due to their better crystallization and the enhancement in the ordering of the carbonate anion in the interlayer. As it observed in Fig. 4A, the vibration mode of CO_3^{2-} species is recorded as a single band because it preserve its D_{3h} symmetry, but should split upon deformation, usually by bonding through one or two of its oxygen atoms, then decreasing the symmetry. Our results show that such splitting is highly evident for sample NiFe15d160, where absorption bands at 1370 and 1350 cm^{-1}, with a shoulder at 1428 cm^{-1}, are recorded, thus indicating a high degree of disorder in the interlayer space of this sample. It has been also observed that such splitting is present in other samples treated at 160° but it was less pronounced at 20 h. This probably be explained that at this time the NiFe LDH sample treated at 160 °C obtain a more order rearrangement. However, all the other samples show a single band centred generally at around 1360 cm^{-1}, indicating that the CO_3^{2-} species have attained a highly symmetric geometry. For iron(III) hydroxides carbonates and some carbonate complexes, a splitting of doubly degenerate asymmetric valence vibration ν_3 of the carbonate group, due to coordination with the metal cations, is observed and a new band at 1500–1650 cm^{-1} appears [38]. The lowering of the carbonate group symmetry can be interpreted as being due to the partial destruction of the anionics layers and direct coordination with metal cations. The bands at low frequency region (below 1000 cm^{-1}) are related with Fe–O, Ni–O and and metal–oxygen–metal vibrational modes in brucite-type layer. The band (out-of-plane deformation) of interlayer carbonate species are also recorded at 840 cm^{-1} (Fig. 4B). The shoulders at 963 and 960 cm^{-1} has been ascribed to the presence of hydroxyl groups [37], while other bands in the 800–400 cm^{-1} range are due to lattice vibrations, mainly involving translational of oxygen ions in the layers. The bands at 730 and 740 cm^{-1} are assigned to the M–OH translation while the bands at 525 and 553 cm^{-1} are assigned to the translation modes of hydroxyl groups, influenced by trivalent cation [39]. The band found around 450–490 cm^{-1} correspond to ν(NiO) vibrations [40]. With regard for the ν_{OH} mode ranging of 4000 and 3000 cm^{-1}, some differences can be also observed in the behavior of different samples. The position of the maximum shifts towards larger wave-numbers as the sample is hydrothermally treated at the same temperature for prolonged time, from 3439 for NiFe4d100 to 3449 cm^{-1} for NiFe7d100, and towards lower wave-numbers as the sample is hydrothermally treated at the lower temperature for the same time (3429 cm^{-1} for NiFe4d85). But for the samples NiFe15d100 and the others treated at high temperature for various time, the spectrum clearly shows a split band around 3500 cm^{-1}. The position of this absorption band at 3500 cm^{-1} should be controlled by cation to which the hydroxyl group is bonded, and if the different types of M–OH moieties exist, the band should be wider or should split [15]. The development of this band around 3500 cm^{-1} upon hydrothermal treatment at high temperature and time should be ascribed to a better defined structure of the OH groups because of the improved crystallinity of the materials. Nevertheless, for the sample treated at 160 °C for 15 days (NiFe15d160), more impurities was observed, which decrease crystallinity. The results depicted in Fig. 4B show that such splitting is highly evident for sample NiFe15d160, where an absorption bands at 3634 and 3568 cm^{-1}, a weak band at 3447 cm^{-1} and two weaker bands at 3245 and 2930 cm^{-1} are recorded. The shift towards lower wave number in our materials should be due to a lower electron density of the O–H bond in hydroxyl groups bonded to Fe^{3+} cations, because of the larger polarizing effect of the trivalent cation [41]. This feature was shown in the spectrum for pure $Al(OH)_3$ [41]. The presence

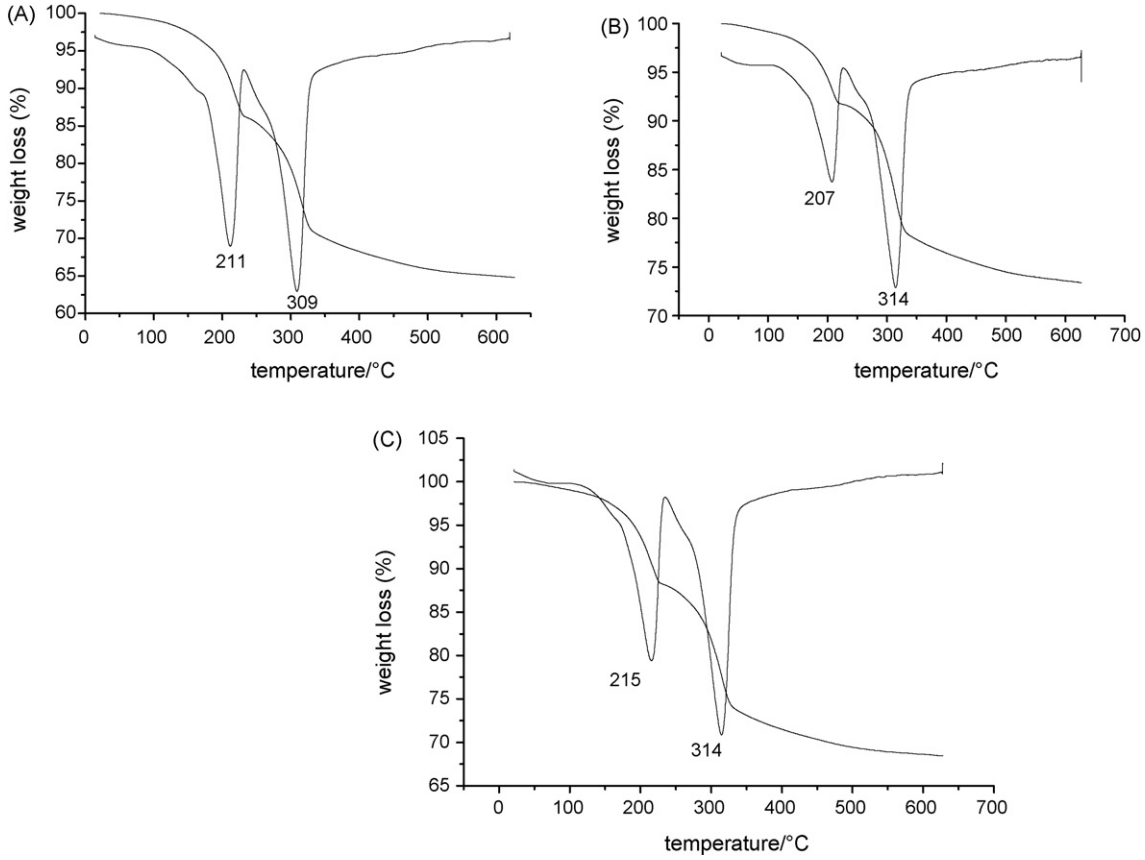

Fig. 5. TG/DTG profiles of $NiFeCO_3$ LDH at different hydrothermal treatment temperatures and times: (A) NiFe15d120, (B) NiFe15d160 and (C) NiFe12d180.

of the band around 3634 cm^{-1} is an indication of the presence of free OH group (Fig. 4B).

The band at 2937 cm^{-1} has been ascribed to water molecule hydrogen-bonded to carbonate ions in the interlayer [6,15,42] (Fig. 4A). It has been noted that this band shift towards higher wave number upon hydrothermal treatment at high temperature and time, indicating that the formation of water-carbonate linkages is evident in the materials where the CO_3^{2-} moiety seems to attain a more symmetric structure, thus accounting for the single band at 1360 cm^{-1}. On the contrary for sample NiFe15d160, where the impurity phase increase gives rise to a more disordered structure, giving rise to CO_3^{2-} species in low symmetry, thus accounting for the split vibration mode at 1428 and 1350 cm^{-1} [43], the interaction with water molecules being non-specific, and thus accounting for the badly resolved and low absorption at 2930 cm^{-1} (Fig. 4B). Thus it has been conclude that the high intensity of this band (Fig. 4A) supposes an important hydration of this compound than NiFe15d160 sample (Fig. 4B). The bands at low frequency region (below 1000 cm^{-1}) are due to other modes of carbonate species and to vibrations implying M–O, M–O–M and O–M–O bonds in brucite-type layer.

3.3. Thermal analysis

Fig. 5 shows a DTA/TG thermogram of the $NiFeCO_3$ materials hydrothermally treated at various temperature and time. All the samples behaved similarly during the thermal study. Two prominent endothermic peaks (at 210 and at 310 °C) are seen in the DTA curve and they were both assigned to the elimination of water and CO_2, respectively. Two weight loss stages were observed for $NiFeCO_3$ in the TG curve, coinciding with two endothermic peaks in the DTA profiles. The first weight loss at 210 °C was ascribed to the loss of physically absorbed and interlayer water and the second weight loss in the temperature range from 240 to 600 °C could be attributed to removal of CO_2 from the interlayer carbonate anions and water molecules from condensation of hydroxyl groups from the brucite-like layers [33,44], thus leading to the destruction of hydrotalcite structure and the formation of mixed $M^{II}_xM^{III}_yO_z$ oxides. Then the material becomes an amorphous metastable mixed solid oxide. The total weight loss of the pure samples in the temperature range up to 600 °C is approximately 35% (Fig. 5A), which corresponds to the sum of water and carbonate contents. On the other hand, the total weight loss of the samples NiFe15d160 and NiFe12h180 are approximately 26 and 31% respectively (Fig. 5B and C). The position of the first peak coincides with the first weight loss recorded in the TG diagram between 20 and 232 °C, which represents 14% for NiFe15d120 sample (Fig. 5A) but for samples NiFe15d160 and NiFe12h180 the first peak coincides with the first weight loss recorded in the TG diagram between 20–227 and 20–235 °C, which represent 8 and 12% respectively (Fig. 5B and C). The second DTA peak should be ascribed to the weight loss recorded between 227 °C up to 600 °C, which represent 20–22% for NiFe15d120 pure hydrotalcite and 18–19% for samples treated at 160 and 180 °C for prolonged times. All the products give the same DTA/TG profile, which indicates that the peak locations are insensitive to the variations in the crystallinity during the hydrothermal treatment conditions [45]. When, comparing all samples and the three samples (Fig. 5), it can be observed that while the second endothermic effect seems to be about the same in all cases, the first endothermic effect is much sharper for sample NiFe15d120 (Fig. 5A), (the same case is observed for NiFe-100 and NiFe-120 at different times), than

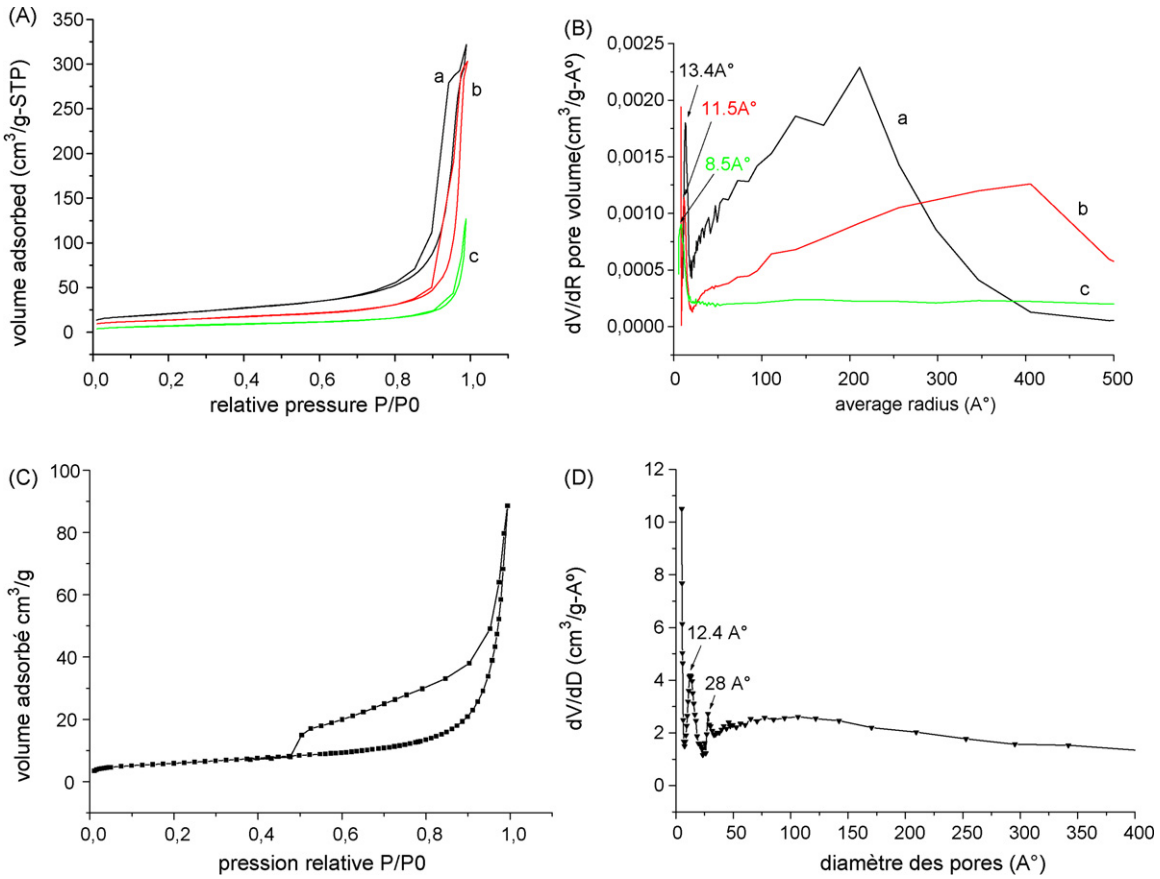

Fig. 6. N_2 adsorption–desorption isotherms (A and C) and pore size distribution (B and D) of [NiFeCO3] LDH treated: for 4 days (A and B) at :(a) 85 °C, (b) 100 °C and (c) 140 °C; for 15 days (C and D) at 160 °C.

for samples treated at 160 and 180 °C for prolonged time (Fig. 5B and C). These latter present the weak reduction in intensity in the first endothermic effect. It is probably due to the larger amount of the amorphous phase and to the decrease of the relative concentration of $NiFeCO_3$ LDH with the time of the treatment in the analyzed product. So we can probably ascribe this endothermic effect to change in the LDH structure. The same effect is also observed in the decrease in the total weight loss which is more marked for the sample NiFe15d160 (26%) as well as the decrease of the temperature range of the first endothermic effect (20–227 °C), probably, due that at higher hydrothermal temperature and time the amorphous phases have led to decrease crystallinity and purity of the samples, thus decreasing the temperature range for water removal. It is also noted that the marked decrease in the weight loss of water in the interlayer (8%) of the sample NiFe15d160 than the other compounds (around 14–15%) is attributed to a less amount of water in this solid. Likewise, the IR spectra (Fig. 4) show the band corresponding (3700–3500 cm^{-1}), and a bending vibrations (around 1630 cm^{-1}) of the interlayer water are more intense in the other samples than NiFe15d160, thus indicating the occurrence of lower amount of interlayer water in this sample.

3.4. Surface area measurements

The effect of hydrothermal treatment temperature and time on the surface area of hydrotalcite samples of Ni/Fe were studied in the range of 85–180 °C. Nitrogen adsorption–desorption isotherms of materials measured at −196 °C are shown in Fig. 6A and the results of surface area measurements are included in Table 3. The shape of all isotherms are type II according to the IUPAC classification [46] and this behavior can be also explained by the existence of spaces between particles of nanometric size thus forming an interparticle porosity. Desorption started immediately after completion of the adsorption (Fig. 6A), which show a narrow hysteresis loop, corresponding to type H3, ascribed to mesopores open at both ends. The slight changes in the hysteresis loops were observed due to the hydrothermal treatment temperature, these changes are related to the shape and homogeneity of the pore size (Fig. 6A). For the samples synthesized at hydrothermal temperature 85 °C, the loops closed around 0.7 relative pressure (P/P_0) with a small plateau at

Table 3
Textural properties of the LDHs precursors and NiFe320 mixed oxides.

Samples	LDH			Samples	LDH		
	S_{BET}[a]	V_p[b]	D_p[c]		S_{BET}[a]	V_p[b]	D_p[c]
NiFe4d85	72	0.49	137	NiFe12h160	33	0.22	132
NiFe4d100	47	0.46	198	NiFe15h160	32	0.19	121
NiFe7d100	50	0.50	201	NiFe20h160	22	0.15	144
NiFe15d100	38	0.40	208	NiFe1d160	32	0.17	110
NiFe4d120	31	0.24	159	NiFe2d160	28	0.18	130
NiFe7d120	27	0.18	268	NiFe4d160	26	0.17	131
NiFe15d120	26	0.22	173	NiFe7d160	25	0.15	123
NiFe4d140	26	0.19	145	NiFe15d160	20	0.13	131
NiFe7d140	25	0.15	122	NiFe3h180	35	0.21	120
NiFe15d140	22	0.20	176	NiFe6h180	23	0.16	136
NiFe3h160	44	0.35	161	NiFe8h180	28	0.17	120
NiFe6h160	38	0.25	133	NiFe12h180	29	0.16	108

[a] Specific surface area (m^2/g).
[b] Cumulative pore volume (cm^3/g).
[c] Pore diameter (Å).

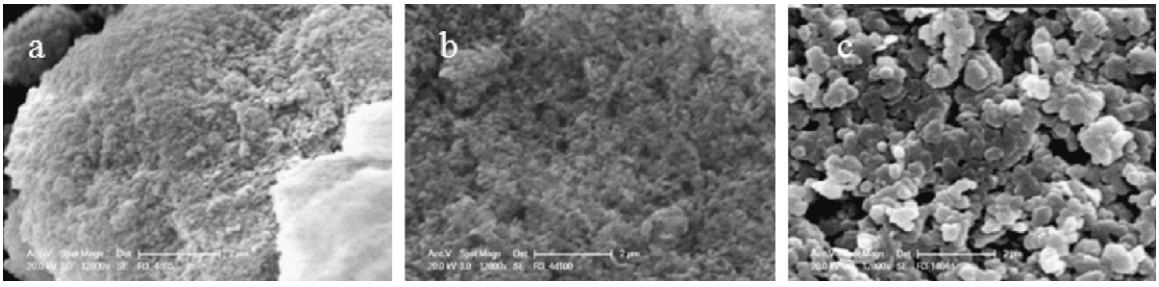

Fig. 7. SEM micrographs of sample [$NiFeCO_3$] hydrothermally treated for 4 days at: (a) 85 °C, (b) 100 °C and (c) 140 °C.

high P/P_0, which attributes to the mesoporous nature of these samples. As the treatment temperature increases, the hysteresis loop closed at P/P_0 around 0.85 and 0.9 for treatment temperature of 100 and 140 °C, respectively. These results indicated that NiFe4d85 had smaller mesopores than NiFe4d100, NiFe4d120 and NiFe4d140. The hysteresis loops (type H3) which exhibit no limiting adsorption at high pressure, are almost vertical and parallel over an appreciable range of relative pressure and such shape of the loops suggests to nonuniform size with aggregates of plate-like particles leading to slit-shaped pores of the hydrotalcite material [47]. The value of average pore volume and surface area for samples treated at 85, 100 and 140 °C are given in Table 3. It can be seen that the surface area was decreased with increasing treatment temperature and time, and thus a much lower adsorption capacity for sample NiFe4d140 is observed, and also in this same sense decreases the width of the hysteresis loop. The pore-size distribution curves of [$NiFeCO_3$] LDH were calculated according to the Barrett, Joyner and Halenda method [28]. It has been shown that the size of the particles is affected by the hydrothermal treatment temperature (Fig. 6B) show a bimodal pore size distribution with an average pore radius centred at 13.4 Å. The pore-size distribution profile of HT-85 and HT-100 samples show a wide distribution with additional pores with a radius of 20 up to 600 Å [Fig. 6B(a) and (b)]. In contrary, HT-140 sample show a monomodal pore size distribution, which is attributed to crystallites growth and aggregation, leading to the disappearance of the voids between crystallites occurred after high treatment temperature. This type of the crystallite growth and aggregation is responsible for the lower specific surface area of the material at higher hydrothermal treatment temperature (Table 3). This feature of pore size distribution is observed starting from the heated temperature of 140 °C. It has been shown that the isotherm feature for sample treated at 160 °C for 15 days (Fig. 6C), and 4–7 days (figure not shown) is different. The hysteresis loop closed at P/P_0 around 0.45 with increasing the width of the hysteresis loop leads to formation of small intraparticle pores. This feature is probably due to the presence of other amorphous phases in addition to hydrotalcite-like sample. It is observed that the pore diameter depends strongly on the heating time (Table 3). Two main tendencies can be drawn from Table 3. First, for a given temperature, in particular for 85 up to 120 °C, the pore diameter increases. Second, at high temperature and prolonged time, in particular for heating temperature 160 °C, the pore diameter decreases first between 3 and 15 h, and increase sharply at 20 h and finally decrease for high duration times. Thus, it can be explained that between 3–15 h and 1–15 days these samples exhibited slightly different intercrystallites packing caused by hydrothermal treatment conditions than the sample treated at 20 h, which presented an abrupt increase in pore diameter. In the same sense, this sample presented an abrupt increase in the diffraction lines intensity (Fig. 3B). After that, for prolonged time the pore diameter and the diffraction lines intensity are varied. It is probably due to the disappearance of the amorphous phase at 20 h indicated by best crystallinity. Then we can conclude that 20 h is the suitable treatment time at 160° for $NiFeCO_3$ at our synthesis conditions.

3.5. Scanning electron microscopy

Scanning electron micrographs of materials hydrothermally treated showed very well crystallized Ni/Fe hydrotalcite-like materials (Fig. 7) emphasize the difference in lateral platelet sizes due to the treatment conditions. It can be observed aggregates of small particles for sample treated at 85 °C (Fig. 7a), by comparison with agglomerated thin spherical-to-hexagonal flat crystals in a layered structure, which is more marked for sample treated at 140 °C (Fig. 7c). SEM images revealed that the hydrothermal treatment temperature and time of the precipitate led to a highly crystalline material having hexagonal platelets. Furthermore, fine granular amorphous phase like agglomerates are dispersed with the NiFe HDL samples treated at 140, 160 and 180 °C for high duration time. It has been observed that the amount of this formed co-product increases with 160 °C for 4–15 days, like demonstrate at above by previous analysis. By comparison with the XRD patterns of samples treated at 160 °C for 1–2 days and at 180 °C for 8–12 h, the amorphous phases are not detected in SEM image. This is due to their lower amount (lower diffraction lines intensity). In addition, the SEM images of the samples treated at 160 °C for 4–15 days and at 180 °C showed agglomeration of primary particles in aggregates (Fig. 8b, d, e, f). These aggregates are formed by strong edge-surface platelet interactions in a so-called “sand rose morphology”, which leads to low surface areas [48]. It is probably result from disordered staking of the particles and the aggregates due to the high treatment temperature and time.

3.6. Transmission electron microscopy

The TEM micrographs show the morphology of regular hexagonal plates, with a thin and wide nature, more or less even, of the Ni/Fe hydroxyl carbonate as shown in (Fig. 9), characteristic of these materials. The size of the particles is affected by the hydrothermal treatment temperature and it was shown that the average size of the lamellar thin hexagonal particles increased with increasing treatment temperature (Fig. 9). The crystallite size varied from 20–150 nm for NiFe4d85 (Fig. 9a) to 200–500 nm for NiFe4d140 (Fig. 9c). TEM images show that at low treatment temperature and time we can see a greater amount of smaller crystallites, which decrease with prolonged time (Fig. 10). This means that with hydrothermal treatment at high temperature and time, predominant growth occurs on the edges resulting in relatively thin, hexagonal plat shaped crystals [12,49]. It can be explained that, the bigger crystallites growing at the expense of smaller one, due to the dissolution, and this process is commonly known as Ostwald ripening. The same observations were found

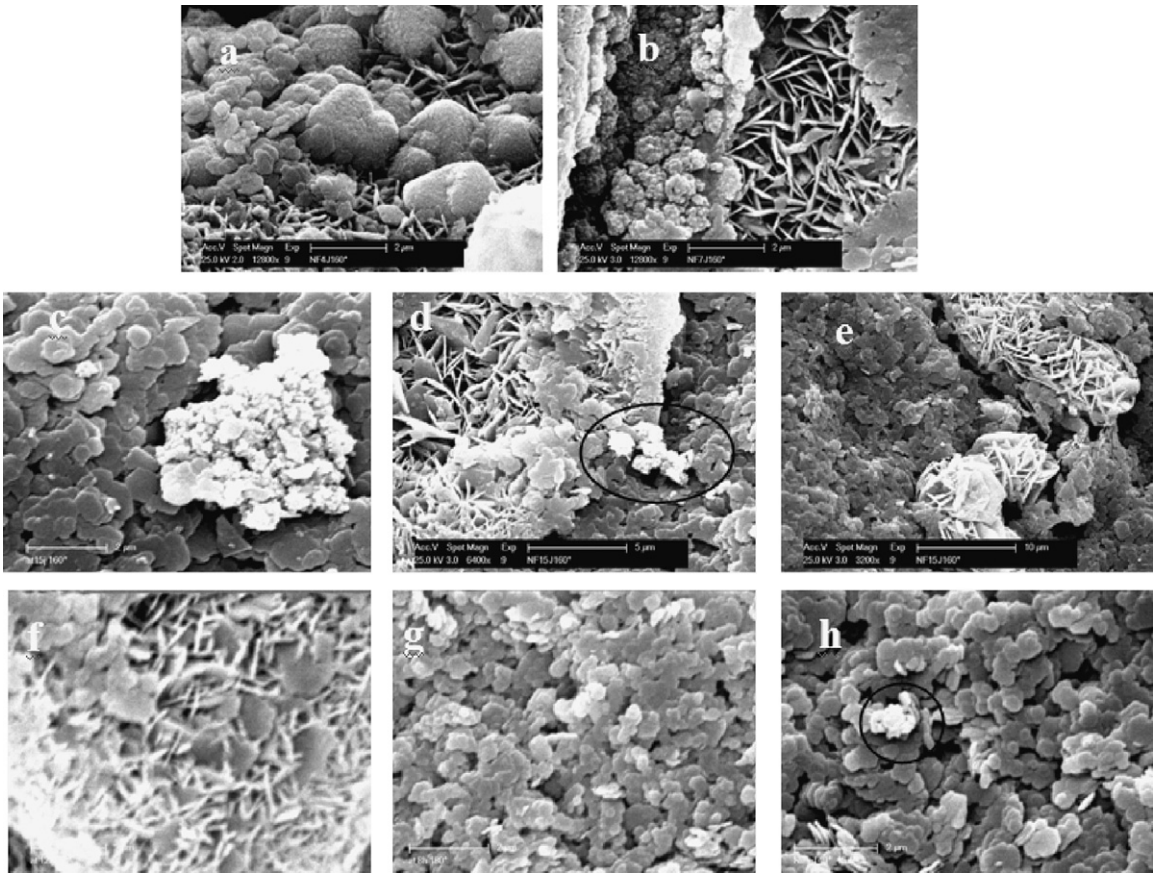

Fig. 8. SEM micrographs of sample [$NiFeCO_3$] hydrothermally treated: (a) 4 days 160 °C; (b) 7 days 160 °C; (c), (d) and (e) 15 days 160 °C, (f) 12 h 180 °C, (g) 8 h 180 °C and (h) 15 days 140 °C. The amorphous phases are surrounded in images (d) and (h).

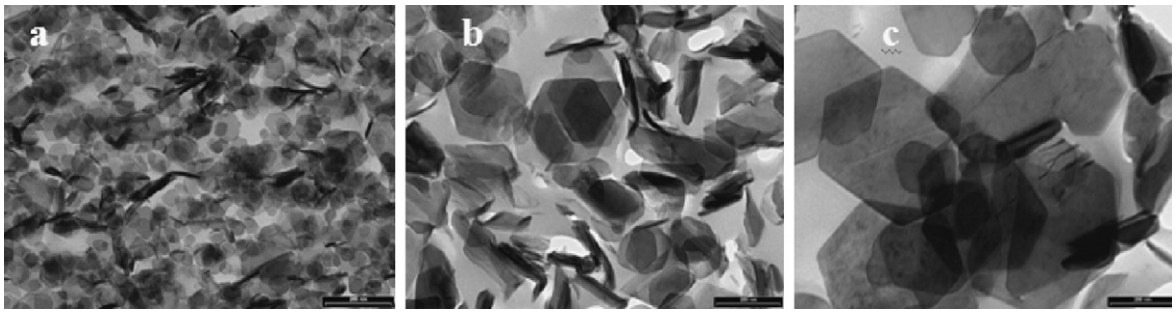

Fig. 9. TEM micrographs of sample [$NiFeCO_3$] hydrothermally treated for 4 days at: (a) 85 °C, (b) 100 °C and (c) 140 °C.

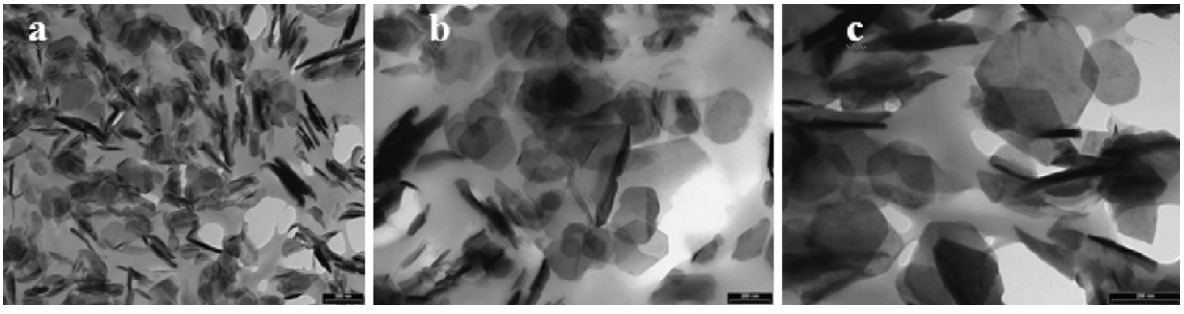

Fig. 10. TEM micrographs of sample [$NiFeCO_3$] hydrothermally treated at 160 °C: (a) 3 h, (b) 12 h and (c) 20 h.

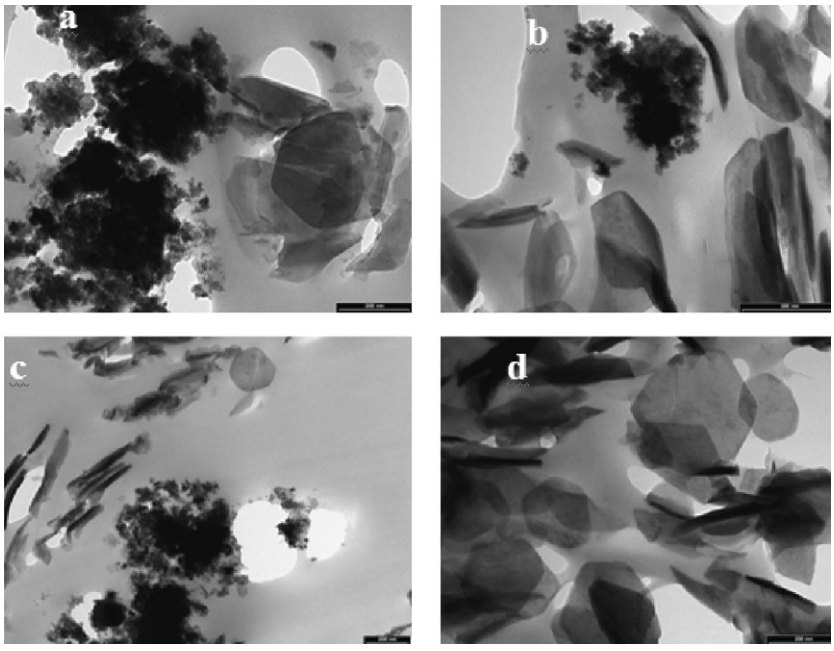

Fig. 11. TEM micrographs of sample [$NiFeCO_3$]; hydrothermally treated at 160 °C for (a) 15 days, (b) 7 days, (c) 4 days, and (d) 20 h 160 °C.

with the MgAl hydrotalcite [36]. This process is more pronounced with prolonged time (Fig. 10). No amorphous phase was noticed in TEM micrographs for sample treated at 85 up to 140 °C indicating the formation of single phase corresponding to hydrotalcite, except for sample treated at 140 °C for 15 days, which was detected at low amount. Furthermore, at hydrothermal treatment at high temperature (160 and 180 °C) and time (1–15 days) were detected an amorphous phases NiO and Ni/Fe oxide (by XRD), which are dispersed and/or agglomerated in fine granular materials in addition to the corresponding hydrotalcite sample, indicating the thermal instability of this material under these conditions (Fig. 11). These phases disappeared at treatment time 20 h, results which entirely confirm by the XRD, IR, and SEM analysis.

3.7. Removal dye performance

The experiments were carried out in order to test the performance of removal Evans Blue dye by adsorption on NiFe LDH according to hydrothermal treatment conditions. Effect of sorption time on EB removal by [$NiFeCO_3$] LDH was examinated at different hydrothermal treatments (Fig. 12). Eq. (1) was used to calculate the color removal efficiency in the treatment experiment:

$$R(\%) = \left[\frac{C_0 - C}{C_0}\right] \times 100 \quad (1)$$

where C_0 and C were the initial and present concentrations of the dye in solution (mg/L), respectively. The results of percent EB adsorption with increasing contact time are presented (Fig. 12), it was found that the EB removal percent increased with increasing contact time. The curves indicate a high dye adsorption rate during the first 2 min and a lower uptake rate there after. Above the 70, 50 and 20% of EB adsorption occurred respectively in the first 2 min for NiFe4d140, NiFe4d100 and NiFe4d85, respectively. Thereafter, the rate of EB adsorption on [$NiFeCO_3$] was found to be slow after 30 min and the equilibrium time was found to be at 45 min. The results showed that the uptake of dye is higher for NiFe4d140 sample, about 95% at the first 15 min than 78 and 40% for those treated at 100 and 85 °C, respectively. So, NiFe4d140 LDH was considerably more efficiency. It is probably due of the sensitive effect of the hydrothermally treatment at high temperature on the structural properties of this adsorbent (see DRX analysis). Fig. 13A also showed that more efficiency adsorption dye was found for sample hydrothermally treated at high temperature for the same time. The curves indicate a high dye adsorption rate during the first 2 min. Above the 72, 66 and 46% of EB adsorption occurred respectively in the first 2 min for NiFe15d160, NiFe15d140 and NiFe15d120, respectively. This feature is probably due to the increase of the particle size with the increase of treatment temperature. Fig. 13B displays that the EB adsorption decrease for NiFe15d160 with very slowly rate than those treated for 4 and 7 days for the same temperature. It can be explained by the presence of more impurities in the first samples (see above) that can influence their adsorption site. The same feature is also shown for samples treated at 180 °C (Fig. 13C). It has been shown that the sample NiFe8h180 has a less dye adsorption and slowly rate adsorption (Fig. 13C(c)) than those treated for 3 and 6 h. However, the contact time required for maximum EB adsorption onto NiFe hydrotalcite was found to be nearly 40 min.

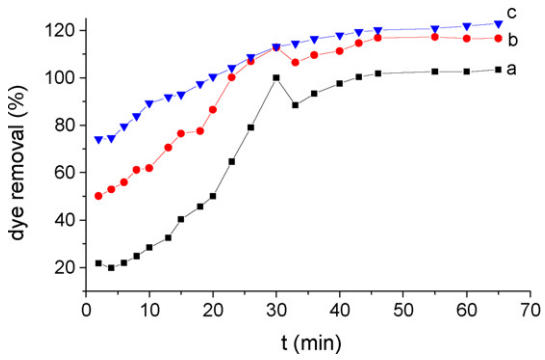

Fig. 12. Effect of hydrothermal treatment on the efficiency of color removal from solution with concentration of the dye = 50 mg/l, of sample [$NiFeCO_3$] treated for 4 days at: (a) 85 °C, (b) 100 °C and (c) 140 °C.

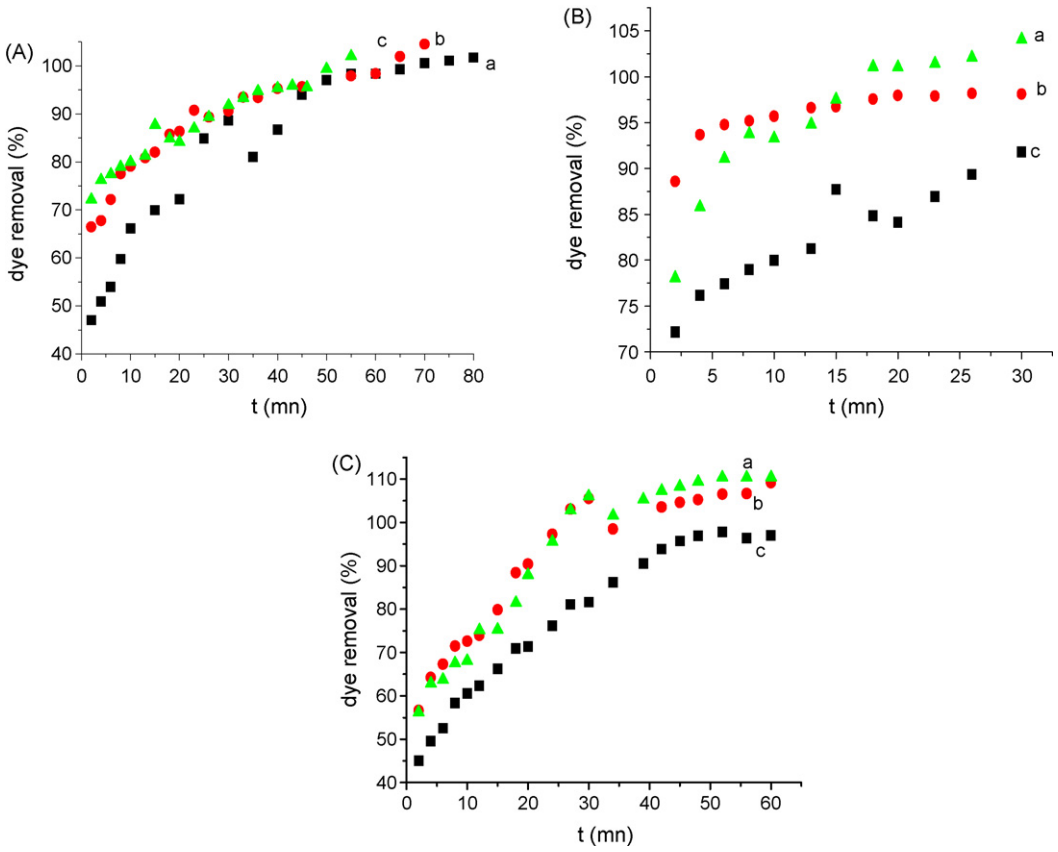

Fig. 13. Effect of hydrothermal treatment on the efficiency of color removal from solution with concentration of the dye = 50 mg/l, of sample [NiFeCO3] treated (A) for 15 days at: (a) 120 °C, (b) 140 °C and (c) 160 °C; (B) at 160 °C for : (a) 4 days, (b) 7 days and (c) 15 days; (C) at 180 °C for : (a) 3 h, (b) 6 h and (c) 8 h.

4. Conclusion

In the present study a hydrotalcite-like material $NiFeCO_3$ with a molar ratio of 3 has been obtained by co-precipitation. The effect of hydrothermal conditions on structural and textural properties was studied in the temperature range 85–180 °C for 3 h–15 days. Hydrothermal treatment leads to a different evolution in the nature of the phases existing in the samples. It should be noted that the materials display the hydrotalcite-type structure. The crystallinity of the samples was observed to increase on increasing the hydrothermal treatment temperature and prolonged time, which gives rise to the decrease of the specific surface area from 74 to 20 m^2/g. Furthermore, amorphous materials are obtained at hydrothermal conditions 140 °C (15 days), 160 °C (1–15 days) and 180 °C (8–12 h), identified by PXRD as the NiO nickel oxide, $Ni(OH)_2$ nickel hydroxide and $NiFe_2O_4$ spinel and by SEM and TEM analysis. Infrared spectra showed a more disordered structure when impurity phases increased. This feature is pronounced for NiFe15d160 sample. Thermal decomposition takes place in two steps: the elimination of water molecules from the interlayer space which occurs around 210 °C, while the second step is due to removal of carbonate anions and hydroxyl groups around 310 °C. The low weight loss percent of water molecules of NiFe15d160 revealed that contain lower amount of interlayer water in this sample and this is in agreement with the infrared results. SEM and TEM results showed an apparent growth of the particles with increasing treatment conditions. A well developed layered and platelet structure of the NiFe hydrotalcite was observed in the SEM image. The average adsorption and desorption pore diameter were observed to be increased on increasing the hydrothermal time. TEM images revealed the regular hexagonal plate's morphology. Our results noticed that the samples treated at 160 and 180 °C tended to yield pure and more crystalline compounds at treatment time 20 and 6 h, respectively.

In an attempt to improve the dye adsorption performance on our materials, we have studied the adsorption capacity according to hydrothermal treatment conditions. It can be seen that the NiFe LDH can be used effectively for the removal of Evans Blue dye from aqueous solutions and the percentage eliminated was found to depend on the hydrothermal treatment conditions of the adsorbent and the contact time. The NiFe LDH was able to remove 45 up to 90% of dye from solutions concentration of 50 mg/l at the first 2 min, according to hydrothermal treatment conditions.

Acknowledgements

The author thanks Algerian government for the scholarship financial support. Pr. Bao-Lian Su is also gratefully acknowledged. The author is grateful to Marie-France Boulanger and Chantal Mathet-Devignon for TEM analysis.

References

[1] A. Vaccari, Preparation and catalytic properties of cationic and anionic clays, Catal. Today 41 (1998) 53–71.
[2] S.K. Yung, T.J. Pinnavaia, Water content and particle texture of synthetic hydrotalcite-like layered double hydroxides, Chem. Mater. 7 (2) (1995) 348–354.
[3] J.E. Moneyron, A. de Roy, C. Forano, J.P. Besse, Realization of humidity sensors based on a screen-printed anionic clay, Appl. Clay Sci. 10 (1995) 163–175.
[4] S.M. Auer, R. Wandeler, U. Göbel, A. Baiker, Heterogeneous coupling of phenylethyne over Cu–Mg–Al mixed oxides—influence of catalyst composition and calcination temperature on structural and catalytic properties, J. Catal. 169 (1997) 1–12.
[5] F. Basile, L. Basini, M.D. Amore, G. Fornasari, A. Guarinoni, D. Matteuzzi, G. Del Piero, F. Trifirò, A. Vaccari, Ni/Mg/Al anionic clay derived catalysts for the cat-

alytic partial oxidation of methane residence time dependence of the reactivity features, J. Catal. 173 (1998) 247–256.
[6] E.C. Kruissink, L.L. van Reijen, J.R.H. Ross, Coprecipitated nickel–alumina catalysts for methanation at high temperature. Part 1. Chemical composition and structure of the precipitates, J. Chem. Soc., Faraday Trans. I 77 (1981) 649–663.
[7] J.M. Oh, M. Park, S.T. Kim, J.Y. Jung, Y.G. Kang, J.H. Chong, Efficient delivery of anticancer drug MTX through MTXLDH nanohybrid system, J. Phys. Chem. Solids 67 (2006) 1024–1027.
[8] M.Z. bin Hussein, Z. Zainal, A.H. Yahaya, D.W.V. Foo, Controlled release of a plant growth regulator, alpha-naphthaleneacetate from the lamella of Zn–Al-layered double hydroxide nanocomposite, J. Control. Release 82 (2002) 417–427.
[9] L. Desigaux, M.B. Belkacem, R. Richard, J. Cellier, P. Leone, L. Carion, F. Leroux, C. Taviot-Gueho, B. Pitard, Selfassembly and characterization of layered double hydroxide/DNA hybrids, Nano Lett. 6 (2006) 199–204.
[10] L. Perioli, V. Ambrogi, B. Bertini, M. Ricci, M. Nocchetti, L. Latterini, C. Rossi, Anionic clays for sunscreen agent safe use: photoprotection, photostability and prevention of their skin penetration, Eur. J. Pharm. Biopharm. 62 (2006) 185–193.
[11] T. Kawabata, Y. Shinozuka, Y. Ohishi, T. Shishido, K. Takaki, K. Takehira, Nickel containing Mg–Al hydrotalcite-type anionic clay catalyst for the oxidation of alcohols with molecular oxygen, J. Mol. Catal. A: Chem. 236 (2005) 206–215.
[12] W.T. Reichele, Synthesis of anionic clay minerals (mixed metal hydroxides, hydrotalcite), Solid State Ionics 22 (1986) 135–141.
[13] M. Lal, A.T. Howe, Studies of zinc–chromium hydroxy salts. I. Thermal decomposition of $[Zn_2Cr(OH)_6]X{\cdot}nH_2O$, where X- = F^-, Cl^-, Br^-, I^-, $1/2CO_3^{2-}$ and NO_3^-, J. Solid State Chem. 39 (1986) 368–376.
[14] T. Lopez, P. Bosch, E. Ramos, R. Gomez, O. Novaro, D. Acosta, F. Figueras, Synthesis and characterization of sol–gel hydrotalcites. Structure and texture, Langmuir 16 (1996) 189–192.
[15] F.M. Labajos, V. Rives, M.A. Ulibarri, Effect of hydrothermal and thermal treatments on the physicochemical properties of Mg–Al hydrotalcite-like materials, J. Mater. Sci. 27 (1992) 1546–1552.
[16] O. Gulnaz, A. Kaya, F. Matyar, B. Arikon, Sorption of basic dyes from aqueous solution by activated sludge, J. Hazard. Mater. 108 (2004) 183–188.
[17] W.T. Tsai, C.Y. Chang, M.C. Lin, S.F. Chien, H.F. Sun, M.F. HSieh, Adsorption of acid dye onto activated carbons prepared from agricultural waste bagasse by $ZnCl_2$ activation, Chemosphere 45 (2001) 51–58.
[18] K. Swaminathan, S. Sandhya, A.C. Sophia, K. Pachhade, Y.V. Subrahmanyam, Decolorization and degradation of H-acid and other dyes using ferrous–hydrogen peroxide system, Chemosphere 50 (2003) 619–625.
[19] A.K. Carlos Gouvêa, F. Wypych, S.G. Moraes, N. Duran, N. Nagata, P. Peralta-Zamora, Semiconductor-assisted photocatalytic degradation of reactive dyes in aqueous solution, Chemosphere 40 (2000) 433–440.
[20] C. O'Neill, F.R. Hawkes, D.L. Hawkes, S. Esteves, S.J. Wilcox, Anaerobic–aerobic biotreatment of simulated textile effluent containing varied ratios of starch and azo dye, Water Res. 34 (2000) 2355–2361.
[21] M.A. Ulibarri, I. Pavlovic, M.C. Hermosin, J. Cornejo, Hydrotalcite-like compounds as potential sorbents of phenols from water, Appl. Clay Sci. 10 (1995) 131–145.
[22] E.L. Crepaldi, J. Tronto, L.P. Cardoso, J.B. Valim, Sorption of terephthalate anions by calcined and uncalcined hydrotalcite-like compounds, Colloid Surf. A: Physicochem. Eng. Aspects 211 (2002) 103–114.
[23] Y. You, G.F. Vance, H. Zhao, Selenium adsorption on Mg–Al and Zn–Al layered double hydroxides, Appl. Clay Sci. 20 (2001) 13–25.
[24] F. Thevenot, R. Szymanski, P. Chaumette, Preparation and characterization of Al-rich Zn–Al hydrotalcite-like compounds, Clays Clay Miner. 37 (1989) 396–402.
[25] Y. You, H. Zhao, G.F. Vance, Adsorption of dicamba (3,6-dichloro-2-methoxy benzoic acid) in aqueous solution by calcined–layered double hydroxide, Appl. Clay Sci. 21 (2002) 217–226.
[26] M.A. Ulibarri, Pavlovic, C. Barriga, M.C. Hermosin, J. Cornejo, Adsorption of anionic species on hydrotalcite-like compounds: effect of interlayer anion and crystallinity, Appl. Clay Sci. 18 (2001) 17–27.
[27] JCPDS: Joint Committee on Powder Diffraction Standards, International Centre for Diffraction Data, Pennsylvania, U.S.A., 1977.
[28] E.P. Barrett, L.G. Joyner, P.P. Halenda, The determination of pore volume and area distributions in porous substances. I. Computations from nitrogen isotherms, J. Am. Chem. Soc. 73 (1951) 373–380.
[29] M. del Arco, P. Malet, R. Trujillano, V. Rives, Synthesis and characterization of hydrotalcites containing Ni(II) and Fe(III) and their calcination products, Chem. Mater. 11 (1999) 624–633.
[30] A. Mendiboure, R. Schollhora, Formation and anion exchange reactions of layered transition metal hydroxides $[Ni_{1-x}M_x]$ $(OH)_2(CO_3)_{x/2}(H_2O)_z$(M = Fe,Co), Rev. Chem. Miner. 23 (1986) 819–827.
[31] A.S. Bookin, V.I. Cherkashin, A. Drits, Polytype diversity of the hydrotalcite-like minerals. II. Determination of the polytypes of experimentally studied varieties, Clays Clay Miner. 41 (1993) 558–564.
[32] A.S. Bookin, A. Drits, Polytype diversity of the hydrotalcite-like minerals. I. Possible polytypes and their diffraction features, Clays Clay Miner. 41 (1993) 551–557.
[33] F. Cavani, F. Trifiro, F. Vaccari, Hydrotalcite-type anionic clays: preparation, properties and applications, Catal. Today 11 (1991) 173–301.
[34] E. Kanezaki, Variable interlayer distance of intercalates of naphthalenedisulfonate isomers in hydrotalcite-like Zn and Al layered double-hydroxides, J. Inclus. Phenom. Mol. Recog. Chem. 24 (1996) 341–351.
[35] P. Kustrowski, D. Sulkowska, L. Chmielarz, A. Rafalska-Lasocha, B. Dudek, R. Dziembaj, Influence of thermal treatment conditions on the activity of hydrotalcite-derived Mg–Al oxides in the aldol condensation of acetone, Micropor. Mesopor. Mater. 78 (2005) 11–22.
[36] L. Hickey, J.T. Kloprogge, R.L. Frost, The effects of various hydrothermal treatments on magnesium–aluminium hydrotalcites, J. Mater. Sci. 35 (2000) 4347–4355.
[37] J.M. Hernandez-Moreno, M.A. Ulibarri, J.L. Rendon, C.J. Serna, IR characteristics of hydrotalcite-like compounds, Phys. Chem. Miner. 12 (1985) 34–38.
[38] K. Nakamoto, Infrared and Raman Spectroscopy of Inorganic and Coordination Compounds, John Wiley, New York, 1978, pp. 283–380.
[39] S. Abello, F. Medina, D. Tichit, J.P. Ramirez, J.C. Groen, J.E. Sueiras, P. Salagre, Y. Cesteros, Aldol condensations over reconstructed Mg–Al hydrotalcites: structure–activity relationships related to the rehydration method, Eur. J. Chem. 11 (2005) 728–734.
[40] E. Uzunova, D. Klissurski, S. Kassabov, Nickel–iron hydroxide carbonate precursors in the synthesis of high-dispersity oxides, J. Mater. Chem. 4 (1994) 153–159.
[41] R.A. Nyquist, R.O. Kagel, Infrared Spectra of Inorganic Compounds, Academic Press, New York, 1971, pp. 206–207.
[42] D.L. Bish, G.W. Brindly, A reinvestigation of takovite, a nickel aluminum hydroxy-carbonate of the pyroaurite group, Am. Mineral. 62 (1977) 458–464.
[43] P. Bento, F.M. Labajos, J. Rocha, V. Rives, Influence of microwave radiation on the textural properties of layered double hydroxides, Micropor. Mesopor. Mater. 94 (2006) 148–158.
[44] V. Rives, Comment on "Direct Observation of a Metastable Solid Phase of $Mg/Al/CO_3$-Layered Double Hydroxide by Means of High-Temperature in Situ Powder XRD and DTA/TG", Inorg. Chem. 38 (1998) 406–407.
[45] S.K. Yun, T.J. Pinnavaia, Water content and particle texture of synthetic hydrotalcite-like layered double hydroxides, Chem. Mater. 7 (1995) 348–354.
[46] K.S.W. Sing, D.H. Everett, R.A.W. Hall, L. Moscou, R.A. Pierotti, J. Rouquérol, T. Siemieniewska, IUPAC Recommendations 1984, Pure Appl. Chem. 57 (4) (1985) 603.
[47] S. Mohmel, I. Kurjawski, D. Uecker, D. Muller, W. Gebner, The influence of a hydrothermal treatment using microwave heating on the crystallinity of layered double hydroxides, Cryst. Res. Technol. 37 (2002) 359–366.
[48] F. Malherbe, C. Forano, J.P. Besse, Use of organic media to modify the surface and porosity properties of hydrotalcite-like compounds, Micropor. Mater. 10 (1997) 67–84.
[49] W.T. Reichele, S.Y. Kang, D.S. Everhardt, The nature of the thermal decomposition of a catalytically active anionic clay mineral, J. Catal. 101 (1986) 352–359.